Photoinduced charge recombination in dipolar D–A–A photonic liquid crystal polymorphs†

Mercedes M. A. Mazza,[a] Shiori Yamazaki,[a] Dieu X. Mai,[a] Suyog Padgaonkar,[a] Samuel Peurifoy,[a] Ariane Goncalves,[a] Yi-Lin Wu,[b] Qiaoyu Hu[a] and Amy M. Scott*[a]

A hexylalkoxy dipolar D–A–A molecule [7-(4-N,N-(bis(4-hexyloxyphenyl)amino)phenyl)-2,1,3-(benzothiadiazol-4-yl)methylene]propane-dinitrile, (C6-TPA-BT-CN) has been synthesized and the photophysics studied via femtosecond transient absorption spectroscopy (FsTA) in toluene and in amorphous and liquid crystalline spherulite thin films. Two spherulite macromolecular crystalline phases (banded, and non-banded) were observed through concentration dependent, solution processing techniques and are birefringent with a negative sign of elongation. A dramatic change in the electronic absorption from blue in amorphous films to green in spherulites was observed, and the molecular orientation was determined through the combined analysis of polarized light microscopy, X-ray diffraction, and scanning electron microscopy. FsTA was performed on amorphous films and show complex charge recombination dynamics, and a Stark effect, characterized from the combined TPA^+ and [BT-CN] spectroscopic signatures at 450 nm and 510 nm and identified through spectroelectrochemistry. Radical cation dynamics of TPA^+ was observed selectively at 750 nm with 4503.3 ps (18%) recombination kinetics resulting in a rather significant yield of free charge carriers in amorphous films and consistent with previous reports on energetically disordered blend films. However, photoexcitation on large, non-banded spherulites areas (4250 mm) reveal average monoexponential charge recombination lifetimes of 169.2 ps from delocalized states similar to those observed in amorphous films and are 5 longer-lived than previous reports [Chang et al., J. Am. Chem. Soc., 2013, 135, 8790] of a related methyl-DPAT-BT-CN whose amorphous thin films were prepared through vapor deposition. Thus, the correlation between the microstructure of the blend film and the photoinduced radical pair dynamics described here is critical for developing a fundamental understanding of how dipolar states contribute to the charge carrier yield in a disordered energy system.

Introduction

Harnessing sunlight as an alternative energy resource con-tinues to stimulate organic photovoltaic (OPV) research with the potential for light-weight, low-cost device fabrication on mechanically flexible substrates.[1] Significant efforts have been devoted towards improving OPV efficiency to reach the Shockley– Queisser limit of 30%;[2] however, challenges still remain to under-stand, control, and ultimately optimize the photon-to-free charge carrier conversion within the photoactive layer. Compared to polymer devices,[3] single-junction bulk-heterojunction devices with efficiencies over 10% are exceptional,[4,5] and small-molecule solution processing for large-scale printing still represents a major challenge. In the typical organic photoactive film,[6] which is comprised of electron donors (D) and acceptors (A), light is absorbed to form an excited state (exciton) that migrates through the solid as an electrically neutral entity. At the interface, the exciton dissociates into geminate radical pairs (or charge transfer state) that are ultimately collected at the electrodes as free charge carriers. Several new classes of small molecules consisting of D–A[7], A–D–A[8], D–A–A, D–A–D, and D–A–p–A[9] conjugated heterocycles with tailored branching,[10] end group functionalization and chain length,[11] and tunable HOMO–LUMO levels have achieved superior performance in OPVs. Furthermore, such chemical structures contain large ground state dipole moments and have been the subject of several investigations to facilitate charge separation at the D:A interface.[12] In short p systems (o4 nm) were D and A are covalently linked and are the majority of systems used in OPVs, electronically coupled D and A units create a unique combination of locally excited (LE) and internal charge transfer (ICT) states. Thus, the energy of the radical pair state created upon photo-excitation directly into the ICT state, [D^{d+}–A^{d}], can be precisely

[a]Department of Chemistry, University of Miami, 1301 Memorial Drive, Coral Gables, FL 33146, USA. E-mail: amscott@miami.edu
[b]Department of Chemistry, Northwestern University, Evanston, IL 60208, USA

determined through direct spectroscopic investigations and the subsequent charge separation at the interface with terminal acceptors undergo a charge shift, where the penalty for nuclei reorganization ($l_{internal}$) around the charge has been precisely determined and overcome.[13] The D–A architecture has also been the subject of decades of research on charge transport within covalent D–bridge–A units, where photoinduced charge, energy, and electron spin transport has been studied extensively in solution, to the extent where semiclassical Marcus Theory[14–17] can predict photoinduced radical pair dynamics in solution[18–20] and more recently in the solid state.[21] However, the performance of these materials in OPVs is ultimately affected by multiple, intertwined variables including materials selection, processing conditions, and device architecture. Naturally, this complicated scenario poses significant challenges to achieving optimized high performance devices. In particular, the correlation between the microstructure of the blend film and the photoinduced radical pair dynamics is critical for such a performance enhance-ment but is poorly understood for all but the most heavily studied systems.[22,23]

Charge transport within liquid crystalline molecules has been examined over the past several decades for implementa-tion in organic-based devices, such as light emitting diodes,[24] thin film transistors,[25] and more recently, OPVs.[26] In high-speed printed devices, performance is limited by reproducibility because BHJ photoactive layers are typically on the order of 80–120 nm and are not consistently pinhole-free. Thus, increas-ing the film thickness above 200 nm typically results in a significant loss in photocurrent because of exciton annihilation and radical pair recombination. Sun and coworkers[27] have reported a molecular nematic liquid crystal (LC) producing an OPV device efficiency of 9.3% with an active layer up to 400 nm using terthiophene rhodamine (BTR) with precisely positioned solubilizing side-chains. Therefore, soluble D–A structures have the potential to behave as nematic liquid crystalline materials and have received very little scrutiny with respect to their photo-physical properties in the solid-state. Recent PCE for vacuum deposited films composed of methyl-TPA-BT-CN:$PC_{71}BM$ films have reached 9.6% efficiency by Forrest and Thompson[28] – a near doubling of efficiency from the initial report by Wong and coworkers[29,30] in 2011. The photophysics was studied by Schaller and Wong[31] in vapor-deposited films and show that charge recom-bination occurs in B33 ps in the neat methyl-DPAT-BT-CN film and that 20% of photogenerated population fail to undergo charge separation to the terminal electron acceptor. However, the question still remains whether the charge recombination[32] dynamics are too fast for unity charge separation and subsequent charge separation to blended electron acceptors in dipolar D–A–A molecules. Here, a hexylalkoxy dipolar D–A–A molecule [7-(4-[N,N-bis(4-hexyloxy-phenyl)amino]phenyl)-2,1,3-benzothia-diazol-4-yl)methylene]-propanedinitrile, [C6-TPA-BT-CN] have been synthesized and the photophysics studied via femtosecond transient absorption spectroscopy (FsTA) in toluene and in amorphous and spherulite thin films prepared via drop-casting. Two spherulite macro-molecular crystalline phases (banded, and non-banded) were observed through concentration dependent processing and they are organized edge-on to the substrate surface. FsTA was performed selectively on large, non-banded spherulites areas and reveal mono-exponential charge recombination lifetimes that are 5 longer-lived than previous reports[31] on related methyl-DPAT-BT-CN, whose amorphous thin films were prepared through vapor deposition. Here, we demonstrate that morphologies with crystalline domains where significant D^+ and A delocalization[33–35] occurs from molecular systems, and when ground state dipole moments facilitate the charge separation, are optimal geometries for increasing photoinduced radical pair lifetimes – one of the major energy loss pathways resulting in poor device efficiency.

Experimental section

The synthesis and chemical structural characterization of dipolar [7-(4-[N,N-bis(4-hexyloxyphenyl)amino]phenyl)-2,1,3-(benzothia-diazol-4-yl)methylene]propane-dinitrile (C6-TPA-BT-CN) is described in Section S1 and S2 of the ESI.† Steady-state and time-resolved absorption and photoluminescence measurements were collected in spectroscopic grade toluene in a 1 cm, for steady-state, and 2 mm, for time-resolved spectroscopy, quartz cuvette. For thin film preparation, the glass substrates were first washed with methanol and then exposed to ozone plasma (Harrick-Plasma Cleaner PDC-32 G) for 15 min. A chlorobenzene solution of C6-TPA-BT-CN (40 mg mL ^{1} and 5 mg mL ^{1}) was stirred and heated at 70 1C for 10 min prior to drop-casting on the glass substrates. After drop-casting, the solvent was allowed to slowly evaporate overnight on the bench top at room temperature, resulting in the formation of dark blue amorphous film of C6-TPA-BT-CN molecules. The thin film morphology was characterized immediately and the thin films were stored in light-free, Teflon containers for further study. Two liquid crystalline morphologies (banded and non-banded spher-ulites) were observed with a noticeable color change from blue to green after storing for 15 days in absence of light. The spherulite liquid-crystalline phases were also observed during rotary evapora-tion and can form under a few hours using heating/vacuum conditions. To further explore this observation, the spherulite thin films were dissolved in toluene and a UV-Vis spectrum showed no apparent chemical degradation.

The steady-state absorption spectra were recorded on a Shimadzu 1800 UV spectrophotometer. The measurements were performed in spectroscopic grade toluene and were con-ducted at room temperature. Optical and polarized light micro-scopy (PLM) images were acquired on an Olympus BX53 microscope with a Linkam thermal stage. Atomic force micro-scopy (AFM) measurements where recorded on a Park System XE 150 Scanning probe microscope operated in non-contact mode with PPP-NCHR 10 M non-contact probes. Scanning electron microscopy (SEM) images were collected on a Hitachi S4800-II cFEG or Hitachi SU8030 SEM at 1.5–5 kV accelerating voltage. The samples were deposited on Al stubs and coated with Au/Pd (10 min) in a Denton Desk III TSC Sputter Coater before examined. X-rays diffraction (PXRD) patterns were measured on a Rigaku ATX-G diffractometer (Cu Ka). The powder samples were either deposited on a glass slide (reflective measurement)

or placed in a thin-walled glass capillary tube (Charles-Supper, 0.7 mm o.d., transmission measurement).

Optical transient absorption (TA) measurements were per-formed with an apparatus based on a commercial amplified Ti:sapphire laser system (Spectra-Physics Mai Tai Oscillator (80 MHz) and 5 W Spitfire Ace Amplifier pumped by a 527 nm Nd:YLF Empower laser) operating at 1 kHz and pumps an optical parametric amplifier (OPA, Spectra Physics, Topas) to produce excitation pulses at 400 nm. The power was varied from 200 nJ per pulse for thin films and from 400 to 1200 nJ per pulse for experiments in solution. The pump diameter of B0.2 mm resulted in energy densities of 1.6 10 ^{4} J cm ^{2} on neat films. More details about the FsTA setup are reported in Section S8 of ESI.†

Results and discussion

Steady-state absorption and photoluminescence

The steady-state absorption spectrum of C6-TPA-BT-CN in toluene is shown in Fig. 1A. The electronic absorption maxima are located at (a) 381 and (b) 581 nm. The higher energy band appearing at 381 nm is attributed to the p–p* transition of the triphenylamine (TPA) moiety. The lower energy band centered at 581 nm with stronger intensity is assigned to intramolecular charge transfer (ICT) from the electron-donating N atom of TPA, where the HOMO level is localized (Fig. 1C), to the electron-withdrawing benzothiadiazole and adjacent dicyano-vinylene groups, where the LUMO is delocalized (Fig. 1C). The comparison of the absorption spectra of C6-TPA-BT-CN, in toluene (blue), and solid states, in the form of 5 mg mL ^{1} thin amorphous film (red) and non-banded spherulite (green), is shown in Fig. 1B. The spectra of the C6-TPA-BT-CN amor-phous and non-banded spherulite films, as compared to the spectrum relative to solution, resulted in broader and red-shifted absorption bands. The different electronic absorption features observed for C6-TPA-BT-CN films arise from aggrega-tion of the molecules, in particular the red-shift indicates the formation of J-type (head-to-tail) aggregation.[36] The aggregation effect on the electronic absorption is more evident in the non-banded spherulite film, where the molecular ordering mimics the common self-assembled 2D polymeric structures in which a mix of J- and H-type of aggregates could exist, crucially affecting the excitons transport mechanisms.[37–39] The large decrease in the intensity of the non-banded spherulite's absorption maximum at 580 nm is due to a strong difference in the optical properties and to the anisotropic nature of the ordered structures.[40]

Optical and morphological study of C6-TPA-BT-CN films

The morphology of C6-TPA-BT-CN films prepared with 5 mg mL ^{1} and 40 mg mL ^{1} solutions, was investigated by X-rays diffraction (XRD), optical and polarized light microscopy (PLM), atomic force microscopy (AFM), and scanning electron microscopy (SEM). Fig. 2A-I shows the optical microscopy image of the dark blue amorphous 5 mg mL ^{1} film and Fig. 2A-II the corresponding polarized light microscopy image. Under ordinary light, the dark blue sample appeared as an amorphous film with no discernable patterns. When the film was observed under crossed polarized light (901 between the polarizer and the analyzer), the dark image of Fig. 2A-II was obtained. This observation, together with the AFM image and height profile (Fig. 2D-I), prove the isotropic nature of the amorphous film, through which the velocity of light or the index of refraction does not change with direction in the substance. This creates a full extinction of the image taken between crossed polarizers.[41] Fig. 2B-I and C-I show the optical microscopy image of the crystalline form of the 40 mg mL ^{1} (banded) and 5 mg mL ^{1} (non-banded) spherulite films, respec-tively, and Fig. 2B-II and C-II the corresponding polarized light microscopy images. Under ordinary light, both films are charac-terized by highly-ordered spherulitic patterns. To obtain informa-tion about the supramolecular ordering of spherulites, the films were investigated using polarized light microscopy. As shown in Fig. 2B-II and C-II, the spherulites of the 5 mg mL ^{1} and 40 mg mL ^{1} films show high birefringence, indicating high aniso-tropy and long-range order. Contrary to the previously described amorphous films, the spherulite molecular packing is characterized by more than one index of refraction and, as a consequence, when the incident plane polarized light enters the birefringent medium, is split into the ordinary (o) and extraordinary (e) rays. The two rays travel through the birefringent medium with diff erent velo-cities and their interference gives rise to the observed color of these films.[41] The observed spherulites consisted of spherically aggregates of crystalline lamellae that radiate from the center

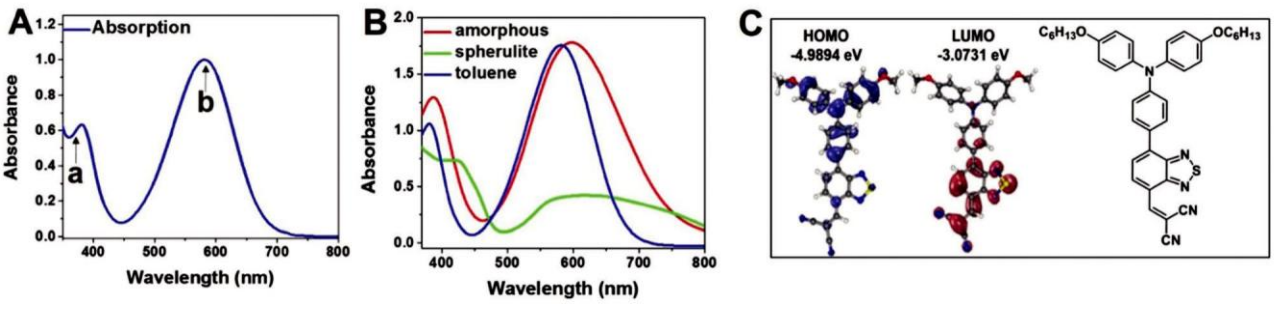

Fig. 1 (A) Absorption spectrum of C6-TPA-BT-CN in toluene: (a) 381 nm, (b) 581 nm. (B) Absorption spectra of C6-TPA-BT-CN in toluene (blue), amorphous film (red), and non-banded spherulite 5 mg mL ^{1} film (green). (C) Frontier molecular orbitals (HOMO and LUMO) calculated with B3LYP/6-31G* Basis Set-Orca software, and molecular structure of C6-TPA-BT-CN.

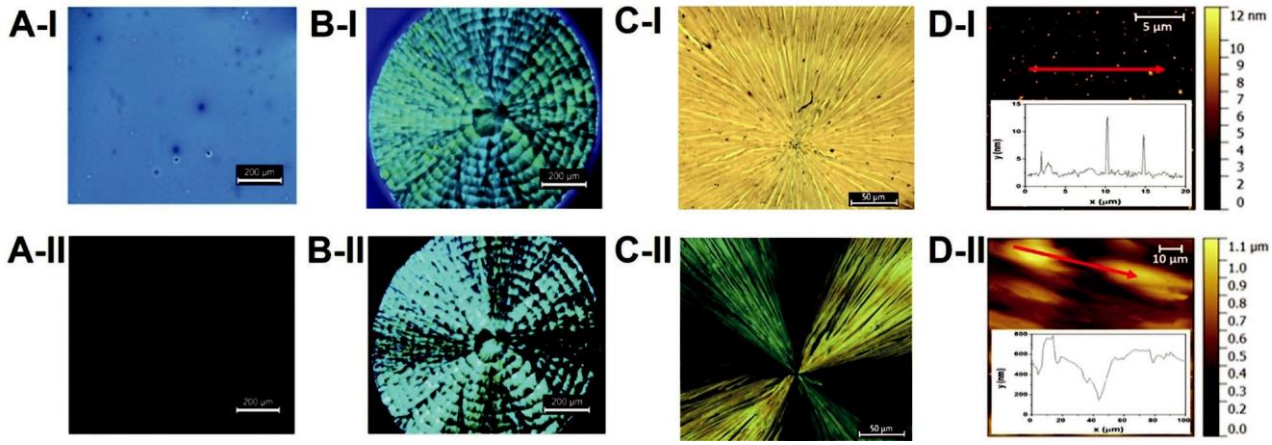

Fig. 2 (A-I, B-I and C-I) Light microscopy images of amorphous, banded spherulite, and non-banded spherulite films. (A-II, B-II and C-II) Polarized light microscopy images of amorphous, banded spherulite, and non-banded spherulite film. (D-I and D-II) Atomic force microscopy images and height profiles (insets) of the amorphous and non-banded spherulite films.

(nucleus) of the spherulite.[42] The existence of the so-called Maltese cross indicates parallel extinction of the lamellae with respect to the direction of polarized light, proving that the lamellae are locally normal to the spherulite radius.[43] However, the polarized light microscopy images of spherulite films pre-pared with the two different concentrations of 5 mg mL ^{1} and 40 mg mL ^{1}, are not identical to each other. In fact, the PLM of spherulite observed on the films prepared with the higher concentration of 40 mg mL ^{1} is characterized by dark concentric rings, alternated to the birefringent rings. The banded pattern was confirmed by scanning electron microscopy as shown in Fig. 3A and B. The use of the lower detector for the SEM analysis allowed to clearly observe clearly the concentric rings of the spherulite. This particular structure of banded spherulite is commonly observed in re-crystallized organic polymers and is found to be concentration and thickness dependent.[44] The extinction rings correspond to zero birefringence and indicate a periodic twisting, re-orientation of the radial lamellae to form helices in which ridges (birefringent rings) and valleys (extinction rings) alternate. Spherulites formed on the 5 mg mL ^{1} films, instead, are categorized as non-banded spherulites composed by a random pattern under PLM of the bright portion of the lamellae with some thin dark areas along the radial direction of spherulites.[45] Also in this structure, the dark spots correspond to extinction positions in which the molecules are normal to the substrate. This observation was confirmed by the AFM image and the corresponding height profile (Fig. 2D-II) where the depletion zone and the height variation from the ridge to the valley is evident. The orientation of the lamellae composing the banded (films from 40 mg mL ^{1} solution) and the non-banded (films from 5 mg mL ^{1} solution) is shown in Fig. 4A and B. In both cases the molecules are edge-on oriented, as confirmed by the negative sign of elongation (Fig. 3C) observed under crossed polarized light when also the first order red compensator was inserted.[43] As shown in Fig. 4C, the molecular packing over the short tangential range (x axes) is given by antiparallel p stacking of the aromatics BT groups, leading to an unusual slip-stacking motif of the molecules that results in a remarkable color change from the blue amorphous film to the green banded spherulite. The described unit is repeated over the long radial range (z axes) allowing the delocalization of the charges over the long-range distance. The amorphous-to-crystalline phase transformation was documented also by XRD. Fig. 3D shows the diffraction pattern collected respectively on the amorphous (bottom graph) and non-banded spherulite 5 mg mL ^{1} film (top graph). The spherulite film exhibited sharp Bragg reflections at 2Y = 3.80901, 11.45901, 15.45901, and 19.10901, suggesting a high degree of crystallinity; whereas the amorphous film displayed an amorphous

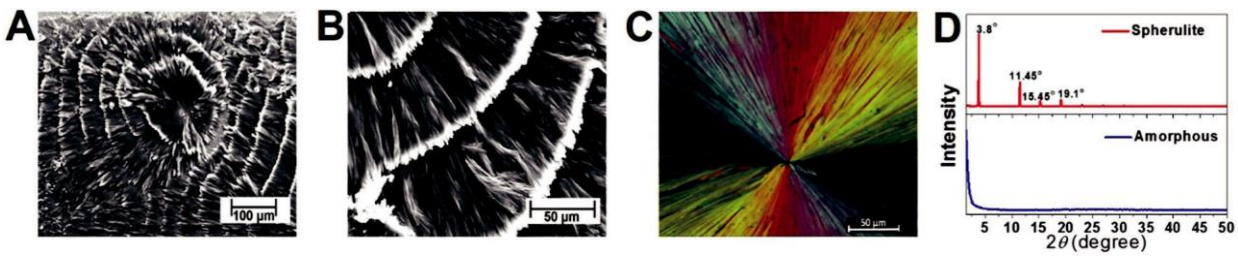

Fig. 3 (A and B) High-resolution SEM images of C6-TPA-BT-CN banded spherulite film collected at different magnifications. (C) Polarized light microscopy image of non-banded spherulite film using a l-plate. (D) X-ray diffraction pattern of C6-TPA-BT-CN spherulite film (red) and amorphous film (blue).

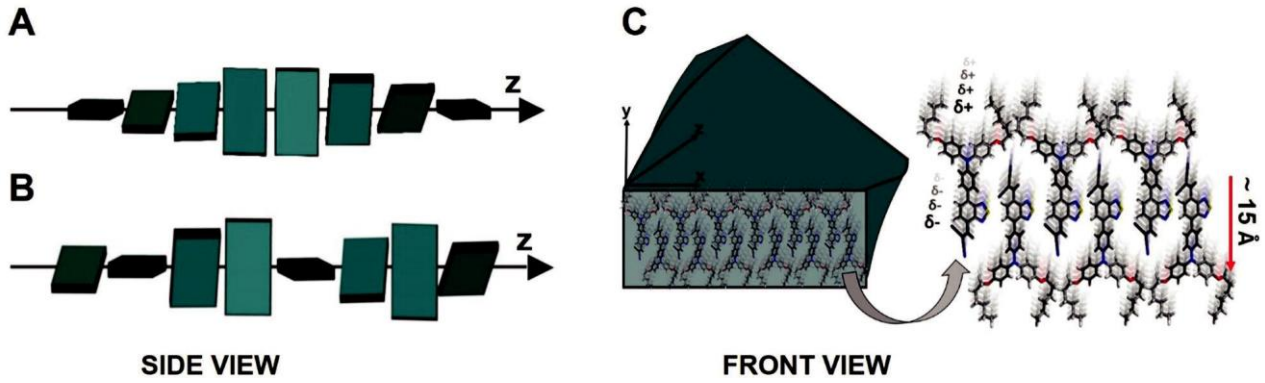

Fig. 4 Side-view representation of lamellar twisting in banded (A) and non-banded spherulite (B). (C) Molecular packing of C6-TPA-BT-CN monomers forming lamellae.

scattering profile. In addition to the out-of-plane diffractions, the spherulite thin film also showed a large number of well-defined diffraction peaks, indicative of 3D crystal packing. Indexing the diffraction peaks with one single set of lattice parameter was unsuccessful, which is likely due to the presence of distinct crystallographic facets.

Transient absorption spectroscopy

The femtosecond transient absorption (FsTA) spectra and kinetics were collected, upon photoexcitation with a B70 fs pulse centered at 400 nm, on C6-TPA-BT-CN in solution and films prepared from 5 mg mL ^{1} solutions. Transient absorp-tion analysis of the films prepared with 40 mg mL ^{1} solution was unsuccessful because the increased thickness of the film produced a very poor ratio of signal to noise. Fig. 5A shows the FsTA spectra obtained of C6-TPA-BT-CN in toluene, recorded between 0 ps and 5 ns time delays. The TA spectra at early delay times, 0 to B13 ps, of C6-TPA-BT-CN in toluene are character-ized by the ground state bleaching (GSB) band centered at 581 nm (b in Fig. 5A) with the formation of two positive features corresponding to excited states absorption (ESA) of a locally excited (LE) state: one weaker (a in Fig. 5A) between 500 and 550 nm and one stronger and broad (c in Fig. 5A) between 600 and 780 nm. With increasing time delay, the GSB band becomes less intense, and at the same time, the ESA at 650 nm strongly increases and slightly shifts to shorter wavelengths. This hypsochromic shift, together with the rise of the ESA, is completed by 13 ps. The transient changes of the rise of ESA at 600 nm is consistent with solvation dynamics of the toluene caused by the dipole moment change of C6-TPA-BT-CN molecules upon S_0 - S_1 excitation. The transient absorption dynamics of C6-TPA-BT-CN in toluene are well represented with

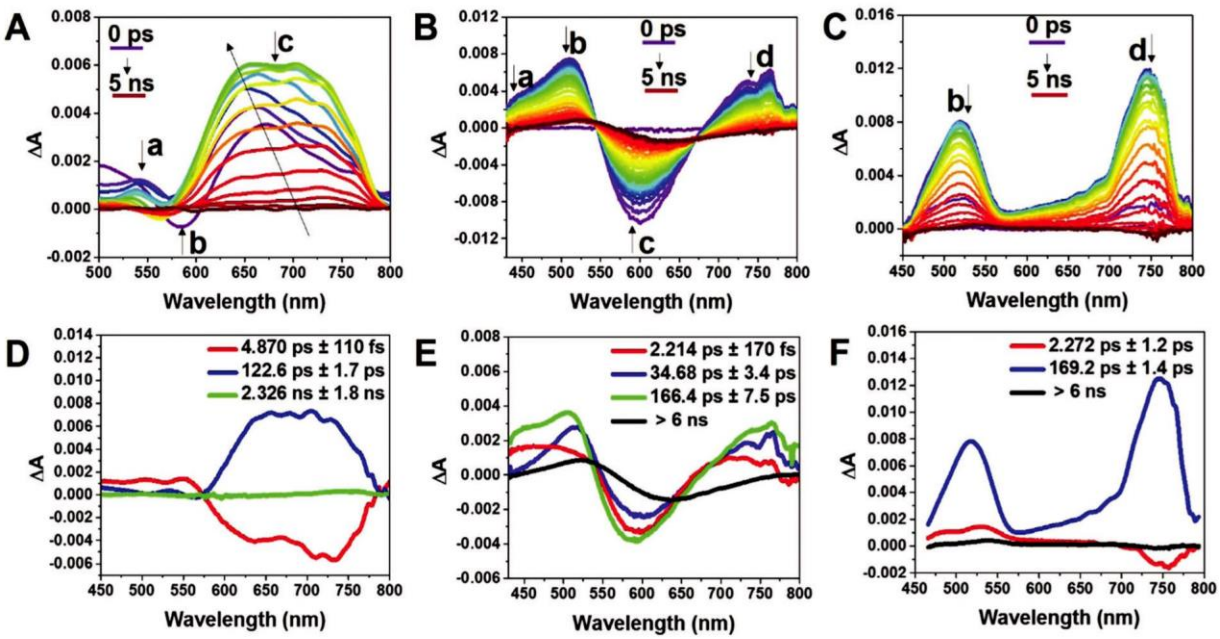

Fig. 5 FsTA spectra of C6-TPA-BT-CN in toluene (A), amorphous (B) and non-banded spherulite (C) films, photoexcited at 400 nm. Global fit analysis of the photoinduced dynamics of C6-TPA-BT-CN in toluene (D), amorphous (E) and spherulite (F) films.

the sum of two exponential functions (Table S2, ESI†). The shortest time constant of 4.6 ps is attributed to intramolecular charge separation (ICS), while the second time constant, 119.4 ps (100%), corresponds to radiative charge recombina-tion (CR). These results are also confirmed by the global fit analysis (Fig. 5D), composed by a shortest charge separation time component of 4.8 ps and a radiative charge recombination time component of 122.6 ps, while the longest component of 2.3 ns is negligible considering the amplitude.

After the FsTA analysis of the sample in toluene, we studied the photoinduced radical pair dynamics of C6-TPA-BT-CN amorphous and spherulite films. Fig. 5B and C, respectively, show the transient absorption spectra of C6-TPA-BT-CN amor-phous and C6-TPA-BT-CN non-banded spherulite films. Photo-excitation of the C6-TPA-BT-CN amorphous film produces transient spectra (Fig. 5B) characterized by three positive bands at 450 (a), 510 (b), and 750 (d) nm that appear within the instrument response time. The GSB band centered at 598 nm
(c) appears slightly shifted to longer wavelengths respect to the corresponding GSB of the sample in toluene (581 nm), match-ing the diff erence observed in the steady-state absorption spectra (Fig. 1B). In addition, the GSB band experiences a gradual red-shift as the time delay increases. This shifting is caused by a first-order Stark eff ect which consists in a change in the optical absorption of ground-state molecules under the
influence of a local electric field generated by photoexcited species.[46] Consistently, as shown in Fig. 6C, the transient spectrum showing the stronger red-shift (red spectrum in
Fig. 6C) perfectly matches the first derivative of the steady-state absorption spectrum.[47,48] The presence of two well dis-tinguished isosbestic points at B540 and 670 nm, represents the superposition of two transient species. Together, the three positive absorption peaks mentioned above (450, 510 and 750 nm) are identical to a diff erence spectrum obtained from spectroelectrochemistry experiments of C6-TPA-BT-CN under oxidizing and reducing conditions (Fig. 6B) and discussed in Section S5 of ESI.† Thus, photoinduced charge separation occurs in the dipolar C6-TPA-BT-CN amorphous film as it does in solution. However, charge separation occurs within our instrument response time and this is discussed and compared with spherulite photophysics later. The transient absorption
spectra with a maximum between 450 (a in Fig. 5B) and 510 (b in Fig. 5B) nm corresponds to ESA of both TPA^+ (a in Fig. 6B) and [BT-CN] (b in Fig. 6B). The band centered at 750 nm (d in Fig. 5B) corresponds to TPA^+ (d in Fig. 6B) exclusively. Selected kinetic traces at the four representative probe wave-lengths of 450 nm (a), 510 nm (b), 581 nm (c), and 750 nm (d), show that each of them fits (Fig. S12, ESI†) with a diff erent set of time constants (Table S3, ESI†). In particular, the charge recombination dynamics of TPA^+ at 750 nm are diff erent compared to those lifetimes fit at 450, 510, and 581 nm and discussed below. The global fit analysis (Fig. 5E) is character-ized by a multiexponential decay with lifetimes of 2.2 ps (14%), 34.7 ps (33%), 166.4 ps (46%) and 46 ns (7%), and are identical to the average lifetimes obtained from the individual kinetics collected at the four representative probe wavelengths. The observed 2.2 ps and 34.7 ps decay components are in agree-ment with literature data reported for amorphous thermally evaporated films based on a related methyl-DPAT-BT-CN molecule.[49] More importantly, the longest decay component of 166.4 ps (46%) indicates a diff erent molecular packing through which the generated radical pairs remain charge separated approximately 5 longer than the previously reported methyl-TPA-BT-CN films. Charge recombination life-times of 4503.3 ps (18%) was observed for TPA^+ at 750 nm and indicate that the radical cation lives 3 longer than the average geminate radical pair [C6-TPA^+ -BT-CN] produced in thin films (166.4 ps) and 4 longer than the intramolecular charge recombination in toluene (122.6 ps). Thus, the rather long-lived TPA^+ ultimately produces free charge carriers in a disordered energetic system is consistent previous work[50] stat-ing that charge separation is efficient in disordered interfaces despite the process occurring in a low dielectric medium. In other work,[51] the femtosecond site-to-site hole hopping (357 fs) obtained for methyl-TPA-BT-CN and observed here suggest that the extensive charge delocalization in TPA units results from a network of highly coupled TPA molecules. Furthermore, the utilization of TPA as a donor, functionalized in the 7 and 4 positions, results in a highly stable TPA^+ whose catalytic self-assembly has been reported in a light-induced reaction with chlorinated solvent. In those systems,[33,34,52,53] TPA units are oxidized and the hydrogen bonded ligands in the periphery of

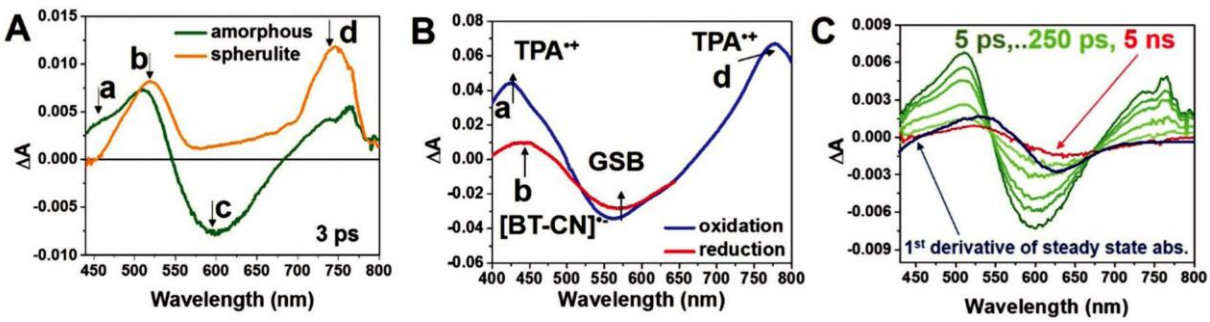

Fig. 6 (A) Overlaid FsTA spectra of C6-TPA-BT-CN amorphous (green) and spherulite (orange) films at 3 ps time delay. (B) Diff erential spectro-electrochemical spectra of C6-TPA-BT-CN oxidation (blue) and reduction (red). (C) FsTA spectra of C6-TPA-BT-CN amorphous film (green and red) and first derivative of the steady-state absorption spectrum (blue spectrum) showing Stark's eff ect.

TPA facilitate planarization of the stable columnar structure, likely with ion–dipole interactions from the chloride counter-ions. Most importantly, hole mobilities in TPA structures are expected to reach as high as 12 cm^2 V^{-1} s^{-1} [33] with delocaliza-tion across 160 TPA units, thus performing as semi-metals.[54] Here, we do not observe such photocatalytic assembly during synthesis or during column chromatography, but the TPA^+ produced during photoexcitation could contribute to a slight planarization and reorganization of TPA and facilitate charge delocalization similar to those assembled photocatalytically. The long-lived TPA^+ lifetimes observed here suggest that new dipolar chemical structures should be designed with different or large surface area accepting groups than BT-CN to facilitate equivalently rapid electron hopping to create extensive delocalized states for improved charge carrier yield in the bulk. These results are in agreement with the general picture[12] that delocalized states at the D:A interface contribute to a higher charge carrier yield because the coulombic energy decreases as the D^+ and A become spatially separated at a critical distance of 4 nm.[50]

Direct photoexcitation of a C6-TPA-BT-CN non-banded spherulite area produces transient absorption spectra reported in Fig. 5C. Two positive, sharp bands dominate the TA spectra, one centered at 520 nm (b in Fig. 5C) and the second one at 750 nm (d in Fig. 5C). In contrast to the TA spectra of C6-TPA-BT-CN amorphous films, the GSB band at 581 nm was not observed in the TA spectra, and this comparison is shown in the overlay spectra in Fig. 6A. The loss of the GSB band in the non-banded spherulites is caused by a decrease in molar extinction coefficient characterized by the molecular packing in the crystalline spherulite, as discussed in the steady state spectroscopy section. In the TA spectral region between 450 and 550 nm, the positive band centered at 520 nm (b in Fig. 5C) corresponds to TPA^+ and [BT-CN] and the band centered at 750 (d in Fig. 5C) is assigned to TPA^+ , from previous spectro-electrochemistry assignments explained above. Selected kinetic traces at the two representative wavelengths of 520 and 750 nm (respectively b and d in Fig. 5C) show that the photoinduced radical pairs are recombining within an average lifetime of 169.5 ps. The kinetic trace obtained through global fit analysis fits well with three lifetime components (Fig. 5F) of 2.3 ps, 169.2 ps and 46 ns. The shortest component of 2.3 ps corresponds to the charge separation, while the 169.2 ps represents the only charge recombination component, and the longest component of 46 ns is negligible in amplitude. Thus, the average geminate recombination of the non-banded spherulites of [C6-TPA^+ -BT-CN] appears to be consistent with 46% of the radical pairs generated in the amorphous film, suggesting that the amorphous films contains small aggregates that grow ‘‘edge-on’’ to the substrate surface and ultimately seed the grow of highly uniform non-banded crystalline spherulites over 100 s of microns in domain size. Further studies are needed to understand the spherulite growth and the influence of TPA units in the self-assembly of the reported polymorphs. Finally, we compare the photophysics of the charge separation in amorphous and spherulite thin films. The photoinduced dynamics of C6-TPA-BT-CN in sperulite and amorphous films within the first 10 ps are different, as shown in the kinetic overlay in the plot of DA vs. log time in Fig. S13 (ESI†). In the amorphous film (blue), charge separation occurs within our instrument response time and we observe a decay with a 2.2 ps lifetime. In contrast, the spherulite film shows a rise within 2 ps (red). These dynamics are consistent with the ground state bleach kinetics. The difference in dynamics is attributed to molecular orientation, where molecules randomly oriented in amorphous films could be interacting through a coulombic interaction in a ‘‘head-to-tail’’ or p stack at van der Waals distances (B3.5 Å), thus leading to ultrafast charge separation and faster intermolecular charge recombination (2.2 ps and 34.7 ps) compared to intra-molecular charge recombination (122.6 ps). Therefore, photo-excitation at 400 nm into the LE state could have more charge transfer character in the amorphous films because of these interactions, also apparent in the drastically different ground state absorptions, as shown in Fig. 1B.

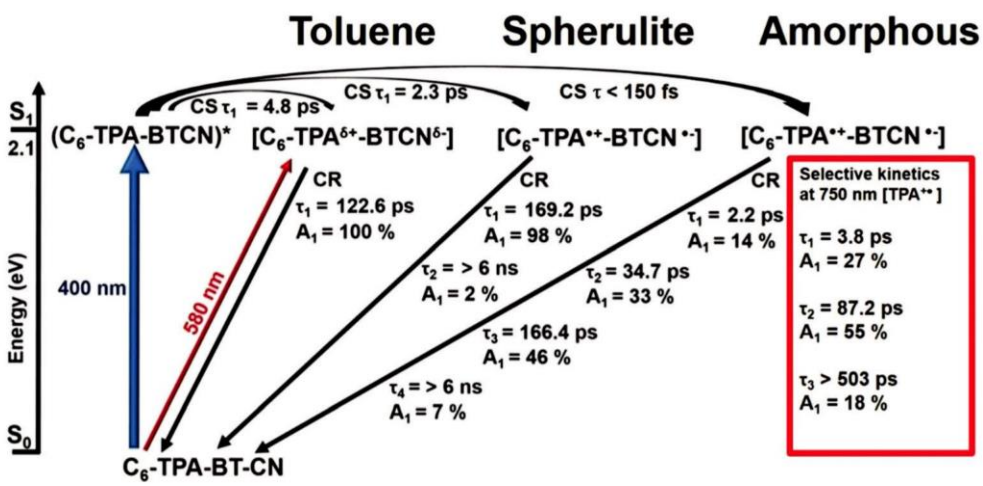

Fig. 7 Jablonski diagram of C6-TPA-BT-CN photoinduced dynamics from global fit and selective kinetics at 750 nm (red box) of amorphous FsTA spectra.

Conclusion

The combination of transient absorption spectroscopy, spectro-electrochemistry, and morphological characterization using XRD, PLM and AFM has offered a deep understanding of the complex photoinduced dynamics of the C6-TPA-BT-CN in solution and in thin film polymorphs, as summarized in the Jablonski diagram in Fig. 7. In the solution-processed amor-phous films, small aggregates created from solution processing and not observed by traditional XRD, grow edge-on to the substrate surface and produce 46% of the radical pair states with a geminate charge recombination lifetime of 166.4 ps. We were able to seed the growth of those aggregates into two spherulite crystalline polymorphs (4250 microns areas) that are birefringent and show a negative sign of elongation. We observed monoexponential charge recombination lifetimes in non-banded spherulites, identical to those in the amorphous film and XRD and PLM ultimately determined their edge-on packing on the substrate. Progressing from solution, through amorphous, to non-banded spherulite films we observed an increase of the TPA^+ and [BT-CN] lifetimes than those reported in methyl-TPA-BT-CN as thermally evaporated amor-phous films. TPA^+ dynamics in amorphous C6-TPA-BT-CN films produce charge delocalized states with a lifetime 3 longer than the geminate pair and ultimately produce long-lived charge carriers (46 ns). We have found that that solution-processed D–A–A dipolar donor materials, whose precise chemical struc-ture is known with simple synthesis and purification, and contain large ground state dipole are an important class of materials for next generation OPVs. From the work outlined here, we suggest that new chemical structures using TPA as a donor has the potential to direct the supramolecular assembly of a D:A interface where the geminate radical cation can ultimately undergo fast hopping between donor sites, which is a key criterion for improving OPV device efficiency.

Author contributions

M. M. A. M., Q. H. and S. Y. conceived and designed the experiments. A. M. S. supervised the project. Q. H. and Syuog P. synthesized the molecules and prepared the films. M. M. A. M. and Q. H. performed the steady-state spectroscopy and PLM characterization and analyzed the data. Q. H. performed the AFM measurement and analyzed the data. D. X. M. and A. G. performed the cyclic voltammetry and spectroelectrochemistry measurements with the help of M. M. A. M. and S. Y. Samuel P. performed the computational analysis. M. M. A. M. performed the FsTA measurements and analyzed the data. Y.-L. W. per-formed the high-resolution SEM and XRD measurements and analyzed the data. M. M. A. M. and A. M. S. wrote the manu-script. All authors discussed the data and contributed to the manuscript.

Competing financial interest

The authors declare no competing financial interests.

Acknowledgements

Y.-L. W. was supported as part of the Argonne-Northwestern Solar Energy Research (ANSER) Center, an Energy Frontier Research Center funded by the U.S. Department of Energy, Office of Science, Office of Basic Energy Sciences under Award Number DE-SC0001059. A. M. S. acknowledges the University of Miami start-up fund for support and the College of Arts & Sciences Convergence grant.

References

1 Y. Sun, G. C. Welch, W. L. Leong, C. J. Takacs, G. C. Bazan and A. J. Heeger, Nat. Mater., 2012, 11, 44.
2 W. Shockley and H. J. Queisser, J. Appl. Phys., 1961, 32, 510.
3 B. G. Kim, E. J. Jeong, J. W. Chung, S. Seo, B. Koo and J. S. Kim, Nat. Mater., 2013, 12, 659.
4 Y. S. Liu, C. C. Chen, Z. R. Hong, J. Gao, Y. Yang, H. P. Zhou, L. T. Dou, G. Li and Y. Yang, Sci. Rep., 2013, 3, 3356.
5 Y. Z. Wu, W. H. Zhu, S. M. Zakeeruddin and M. Gratzel, ACS Appl. Mater. Interfaces, 2015, 7, 9307.
6 S. R. Forrest, MRS Bull., 2005, 30, 28.
7 A. Das and S. Ghosh, Angew. Chem., Int. Ed., 2014, 53, 2038.
8 N. Karakostas, A. Kaloudi-Chantzea, E. Martinou, K. Seintis, F. Pitterl, H. Oberacher, M. Fakis, J. K. Kallitsis and G. Pistolis, Faraday Discuss., 2015, 185, 433.
9 M. Wielopolski, J. H. Kim, Y. S. Jung, Y. J. Yu, K. Y. Kay, T. W. Holcombe, S. M. Zakeeruddin, M. Gratzel and J. E. Moser, J. Phys. Chem. C, 2013, 117, 13805.
10 A. Sharenko, C. M. Proctor, T. S. van der Poll, Z. B. Henson, T. Q. Nguyen and G. C. Bazan, Adv. Mater., 2013, 25, 4403.
11 Z. Guo, D. Lee, R. D. Schaller, X. B. Zuo, B. Lee, T. F. Luo, H. F. Gao and L. B. Huang, J. Am. Chem. Soc., 2014, 136, 10024.
12 H. M. Feier, O. G. Reid, N. A. Pace, J. Park, J. J. Bergkamp, A. Sellinger, D. Gust and G. Rumbles, Adv. Energy Mater., 2016, 6, 502176.
13 G. Nan, X. Zhang and G. Lu, Phys. Chem. Chem. Phys., 2016, 18, 17546.
14 B. Albinsson and J. Martensson, J. Photochem. Photobiol., C, 2008, 9, 138.
15 P. F. Barbara, T. J. Meyer and M. A. Ratner, J. Phys. Chem., 1996, 100, 13148.
16 R. A. Marcus, J. Chem. Phys., 1965, 43, 679.
17 R. A. Marcus, J. Chem. Phys., 1965, 43, 3477.
18 C. X. Guzman, R. M. K. Calderon, Z. Li, S. Yarnazaki, S. R. Peurifoy, C. C. Guo, S. K. Davidowski, M. M. A. Mazza, X. Han, G. Holland, A. M. Scott and A. B. Braunschweig, J. Phys. Chem. C, 2015, 119, 19584.
19 D. Ley, C. X. Guzman, K. H. Adolfsson, A. M. Scott and A. B. Braunschweig, J. Am. Chem. Soc., 2014, 136, 7809.
20 A. M. Scott, T. Miura, A. B. Ricks, Z. E. X. Dance, E. M. Giacobbe, M. T. Colvin and M. R. Wasielewski, J. Am. Chem. Soc., 2009, 131, 17655.
21 S. Spencer, J. Cody, S. Misture, B. Cona, P. Heaphy, G. Rumbles, J. Andersen and C. Collison, J. Phys. Chem. C, 2014, 118, 14840.

22 J. Kirkpartrick, P. E. Keivanidis, A. Bruno, F. Ma, S. A. Haque, A. Yarstev, V. Sundstrom and J. Nelson, J. Phys. Chem. B, 2011, 115, 15174.
23 T. M. Clarke, A. M. Ballantyne, J. Nelson, D. D. C. Bradley and J. R. Durrant, Adv. Funct. Mater., 2008, 18, 4029.
24 C. Y. Xia, X. M. Wang, J. Lin, W. L. Jiang, Y. Ni and W. Huang, Synth. Met., 2009, 159, 194.
25 I. McCulloch, W. Zhang, M. Heeney, C. Bailey, M. Giles, D. Graham, M. Shkunov, D. Sparrow and S. Tierney, J. Mater. Chem., 2003, 13, 2436.
26 L. Schmidt-Mende, A. Fechtenkotter, K. Mullen, E. Moons, R. H. Friend and J. D. MacKenzie, Science, 2001, 293, 1119.
27 K. Sun, Z. Y. Xiao, S. R. Lu, W. Zajaczkowski, W. Pisula, E. Hanssen, J. M. White, R. M. Williamson, J. Subbiah, J. Y. Ouyang, A. B. Holmes, W. W. H. Wong and D. J. Jones, Nat. Commun., 2015, 6, 6013.
28 O. L. Griffith, X. Liu, J. A. Amonoo, P. I. Djurovich, M. E. Thompson, P. F. Green and S. R. Forrest, Phys. Rev. B: Condens. Matter Mater. Phys., 2015, 92, 085404.48 K. Oum, P. W. Lohse, J. R. Klein, O. Flender, M. Scholz,
29 L. Y. Lin, C. W. Lu, W. C. Huang, Y. H. Chen, H. W. Lin and K. T. Wong, Org. Lett., 2011, 13, 4962.
30 L. Y. Lin, Y. H. Chen, Z. Y. Huang, H. W. Lin, S. H. Chou, F. Lin, C. W. Chen, Y. H. Liu and K. T. Wong, J. Am. Chem. Soc., 2011, 133, 15822.
31 A. Y. Chang, Y. H. Chen, H. W. Lin, L. Y. Lin, K. T. Wong and R. D. Schaller, J. Am. Chem. Soc., 2013, 135, 8790.
32 C. M. Proctor, M. Kuik and T. Q. Nguyen, Prog. Polym. Sci., 2013, 38, 1941.
33 E. Busseron, J. J. Cid, A. Wolf, G. Y. Du, E. Moulin, G. Fuks, M. Maaloum, P. Polavarapu, A. Ruff , A. K. Saur, S. Ludwigs and N. Giuseppone, ACS Nano, 2015, 9, 2760.
34 K. Watanabe, H. Iida and K. Akagi, Adv. Mater., 2012, 24, 6451.
35 G. Lugito, E. M. Woo and Y. T. Hsieh, Macromolecules, 2015, 48, 7953.
36 F. C. Spano, Acc. Chem. Res., 2009, 43, 429.
37 J. Sung, P. Kim, B. Fimmel, F. Wu¨rthner and D. Kim, Nat. Commun., 2015, 6, 8646.
38 T. Hasobe, S. Fukuzumi and P. V. Kamat, J. Am. Chem. Soc., 2005, 127, 11884.
39 H. Yamagata and F. C. Spano, J. Chem. Phys., 2012, 136, 184901.
40 L. Garcia-Rubio, Macromolecules, 1992, 25, 2608.
41 W. McCrone, L. McCrone, J. Delly and Mich, Polarized Light Microscopy, 1978.
42 J. L. Hutter and J. Bechhoefer, J. Cryst. Growth, 2000, 217, 332.
43 W. Pisula, M. Kastler, D. Wasserfallen, T. Pakula and K. Mu¨llen, J. Am. Chem. Soc., 2004, 126, 8074.
44 E. M. Woo and G. Lugito, Eur. Polym. J., 2015, 71, 27.
45 A. Toda, Encyc. Polym. Comp., 2013, 978.
46 U. B. Cappel, S. M. Feldt, J. Scho¨neboom, A. Hagfeldt and G. Boschloo, J. Am. Chem. Soc., 2010, 132, 9096.
47 M. Fakis, P. Hroba´rik, O. Yushchenko, I. Sigmundova´, M. Koch, A. Rosspeintner, E. Stathatos and E. Vauthey, J. Phys. Chem. C, 2014, 118, 28509.
A. Hagfeldt, G. Boschloo and T. Lenzer, Phys. Chem. Chem. Phys., 2013, 15, 3906.
49 A. Y. Chang, Y. H. Chen, H. W. Lin, L. Y. Lin, K. T. Wong and R. D. Schaller, J. Am. Chem. Soc., 2013, 135, 8790.
50 S. N. Hood and I. Kassal, J. Phys. Chem. Lett., 2016, 7, 4495.
51 O. L. Griffith, X. Liu, J. A. Amonoo, P. I. Djurovich, M. E. Thompson, P. F. Green and S. R. Forrest, Phys. Rev. B: Condens. Matter Mater. Phys., 2015, 92, 085404.
52 I. Nyrkova, E. Moulin, J. J. Armao, M. Maaloum, B. Heinrich, M. Rawiso, F. Niess, J. J. Cid, N. Jouault, E. Buhler, A. N. Semenov and N. Giuseppone, ACS Nano, 2014, 8, 10111.
53 V. Faramarzi, F. Niess, E. Moulin, M. Maaloum, J. F. Dayen, J. B. Beaufrand, S. Zanettini, B. Doudin and N. Giuseppone, Nat. Chem., 2012, 4, 485.
54 E. Moulin, F. Niess, M. Maaloum, E. Buhler, I. Nyrkova and N. Giuseppone, Angew. Chem., Int. Ed., 2010, 49, 6974.